# Two-Dimensional, Non-Equilibrium Modeling of a Gas Tungsten Arc

Gui-Qing Wu[1], L. G. Benilova[2], He-Ping Li[1,*], M. S. Benilov[2], Xi Chen[3]

[1]*Department of Engineering Physics, Tsinghua University, Beijing 100084, P. R. China*
[2] *Departamento de Física, Universidade da Madeira, Largo do Minicípio, 9000 Funchal, Portugal*
[3]*Department of Engineering Mechanics, Tsinghua University, Beijing 100084, P. R. China*

([*] Corresponding author, H.-P. Li: liheping@tsinghua.edu.cn)

**Abstract:** In this paper, a two-dimensional, two-temperature modeling on the heat transfer and flow patterns of a gas tungsten arc plasma is conducted with a coupled non-equilibrium hydrodynamic and non-linear surface heating model. The modeling results show that the shielding gas flow rate and the position of the shielding gas nozzle exit can influence obviously the arc non-equilibrium characteristics, especially in the arc fringes.

**Keywords:** Two-dimensional; non-equilibrium; modeling; arc; GTA

## 1. Introduction

Due to their outstanding features with rather high specific enthalpy and thermal conductivity, gas discharge thermal plasmas have been used widely in the fields of advanced materials processing. Many studies have been conducted for investigating the effects of different conditions, such as the operation parameters, the plasma-working gases, the electrode materials and shapes, the applied magnetic fields, *etc.*, on the arc characteristics and complex interactions between plasmas and electrodes [1-6]. Among different types of thermal plasma sources, gas tungsten arc (GTA) plasmas have been widely employed in industries for metallic materials welding. In previous studies, the effects on the arc characteristics and the welding qualities have been considered under different operation conditions, such as different electrode materials and shapes, compositions of the plasma-working gas and/or the shielding gas, flow rates, arc currents, *etc.* (*c.f.* [7]). Usually a local thermodynamic equilibrium (LTE) model was employed to study the characteristics of a GTA with shielding gas flowing (*e.g.* [8]). On the other hand, experimental investigations [9] on the DC arcs showed that non-equilibrium effects were pronounced near the electrodes and other cold walls or in the fringe regions of the arc, although the deviation from the LTE state in the arc core region was not significant for high-intensity DC arcs. In Ref. [10], by combining the two-temperature hydrodynamic model for the flow-affected region and the model of non-linear surface heating for the solid cathode and the near-cathode layer regions, the non-equilibrium features of the arc, as well as the energy transfer mechanisms in the cathode sheath region, were simulated.

It is expected that different flow rates of the shielding gas and the positions of the shielding-gas nozzle exit relative to the arc cathode or work-piece in a GTA system would influence the non-equilibrium characteristics of the arc plasmas, especially in the arc fringes. In this paper, a two-dimensional (2D), two-temperature (2T) modeling on the non-equilibrium characteristics of the GTA plasmas with argon as the plasma-forming gas and the shielding gas is conducted by using the numerical method presented in Ref. [10].

## 2. Model descriptions

In the present paper, main assumptions include that (1) in the arc column region, the argon plasma deviates from the LTE state but is in the local chemical equilibrium (LCE) state, *i.e.* the electron temperature ($T_e$) is different from the heavy-particle temperature ($T_h$) and the 2T model can be employed; (2) the plasma flow is quasi-steady and in laminar regime; (3) gravity is neglected as a minor effect; (4) the viscous dissipation and the work of the pressure gradient are negligible due to the small values of the Mach number; (5) the thermodynamic and transport properties of argon plasmas are the functions of the temperatures ($T_e$ and $T_h$) at atmospheric pressure; (6) the plasma is optically thin and (7) the contamination of metal vapor originating from the electrodes is not considered in this study.

### *2.1. Governing equations*

Based on the preceding assumptions, the governing equations in the axi-symmetric, cylindrical coordinates (*r*, *z*) for the flow-affected region are as follows:

Continuity equation:

$$\frac{1}{r}\frac{\partial}{\partial r}(r\rho v_r)+\frac{\partial}{\partial z}(\rho v_z)=0 \qquad (1)$$

Momentum conservation equation (*z*-direction):

$$\rho\left(v_r\frac{\partial v_z}{\partial r}+v_z\frac{\partial v_z}{\partial z}\right)=-\frac{\partial p}{\partial z}+\frac{1}{r}\frac{\partial}{\partial r}\left[\mu r\left(\frac{\partial v_z}{\partial r}+\frac{\partial v_r}{\partial z}\right)\right]+\frac{\partial}{\partial z}\left(2\mu\frac{\partial v_z}{\partial z}\right)+j_r B_\theta \quad (2)$$

Momentum conservation equation (*r*-direction):

$$\rho\left(v_r\frac{\partial v_r}{\partial r}+v_z\frac{\partial v_r}{\partial z}\right)=-\frac{\partial p}{\partial r}+\frac{\partial}{\partial r}\left(2\mu\frac{\partial v_r}{\partial r}\right)+\frac{\partial}{\partial z}\left[\mu\left(\frac{\partial v_r}{\partial z}+\frac{\partial v_z}{\partial r}\right)\right]+\frac{2\mu}{r}\left(\frac{\partial v_r}{\partial r}-\frac{v_r}{r}\right)-j_z B_\theta \quad (3)$$

Energy conservation equation for electrons:

$$\nabla\cdot\left(\frac{5}{2}n_e k_B T_e\vec{v}\right)=\nabla\cdot\left(k_e\nabla T_e\right)+\vec{j}\cdot\vec{E}-U_r+\frac{5}{2}\frac{k_B}{e}\left(\vec{j}\cdot\nabla T_e\right)-\dot{E}_{el} \quad (4)$$

Energy conservation equation for heavy particles:

$$\nabla\cdot\left\{\left[\frac{5}{2}\left(n_a+n_i\right)k_B T_h+n_i E_i\right]\vec{v}\right\}=\nabla\cdot\left[\left(k_a+k_i+k_r\right)\nabla T_h\right]+\dot{E}_{el} \quad (5)$$

where $v_r$ and $v_z$ are the components of the velocity vector $\vec{v}$ in *r*- and *z*-directions, $n$, $T$ and $p$ are the particle number density, temperature and gas pressure, $\rho$, $\mu$, $k$ and $U_r$ are the mass density, dynamic viscosity, thermal conductivity and radiation power per unit volume of plasmas, respectively. $e$ and $k_B$ are the elementary charge and the Boltzmann constant, $E_i$ is the ionization energy. The subscripts $h$, $e$, $a$ and $i$ represent heavy particle, electron, atom, and singly-ionized ion, respectively. All the thermodynamic and transport properties of argon plasmas are functions of the temperatures ($T_e$ and $T_h$) at atmospheric pressure. The reactive thermal conductivity, $k_r$, has been included in the heavy-particle energy equation (5) [10, 11]. $\vec{j}$ and $\vec{E}$ are the current density vector and the electric field vector, respectively. $B_\theta$ is the self-induced magnetic field in the circumferential direction. $\dot{E}_{el}$ is the energy transferred in elastic collisions between electrons and heavy particles, which is expressed as

$$\dot{E}_{el}=\left(2m_e/m_h\right)\left(\bar{\nu}_{ea}+\bar{\nu}_{ei}\right)n_e\left[\left(3/2\right)k_B\left(T_e-T_h\right)\right] \quad (6)$$

where $\bar{\nu}_{ei}$ and $\bar{\nu}_{ea}$ are the averaged electron-ion and electron-atom collision frequencies [12, 13], $m_e$ and $m_h$ are the masses of the electrons and heavy particles, respectively.

Due to the passage of the current in the arc column region, the electric potential equation

$$\nabla\cdot\left(\sigma\nabla\phi\right)=0 \quad (7)$$

will be solved, where $\sigma$ is the electric conductivity, $\phi$ is the electric potential which relates to the electric field as $\vec{E}=-\nabla\phi$. The current density is calculated from $\vec{j}=\sigma\vec{E}$, and $B_\theta$ is calculated by $B_\theta=\left(\mu_0/r\right)\int_0^r j_x\xi d\xi$.

No flow exists inside the anode region if the flows of the molten metals are neglected. Thus, only the heat conduction equation and current continuity equation are necessary in the solid anode region, *i.e.*

$$\nabla\cdot\left(k_m\nabla T\right)+\vec{j}\cdot\vec{E}=0 \quad (8)$$

$$\nabla\cdot\left(\sigma_m\nabla\phi\right)=0 \quad (9)$$

where $k_m$ and $\sigma_m$ are the thermal conductivity and electric conductivity of the anode material (copper), physical properties of which are take from [14].

In this study, the additional energy flux from the arc column to the anode surface is given by [15]

$$q_{pa}=\left|\vec{j}\right|\left(W_a+2.5\frac{k_B}{e}Te\right) \quad (10)$$

where $W_a$ is the work function of the anode material ($W_a$ =4.65V is employed in this study [15]). After multiplying by the surface area of the pertinent near-surface control volume, and then, dividing by its volume, $q_{pa}$ will be added to the near-surface control volume on the anode side as the additional source term in the energy equation (8).

In this paper, the tungsten cathode solid region and the near-cathode plasma layer are simulated by means of the model of non-linear surface heating [16, 17], and coupled with the 2T hydrodynamic model for the flow affected region as that presented in Ref. [10].

### *2.2. Calculation domain and boundary conditions*

The calculation domain with the geometrical dimensions for this modeling is shown in Fig. 1, which includes the solid electrode (cathode and anode) regions, the near-cathode layer and the arc column region (MCDEFGHIJAM). The cathode (tungsten) is composed of a cylinder and a semi-sphere with radius of 1.0 mm. The total length of the cathode is 12.0 mm, while the distance between the cathode frontal surface and the anode inner surface is fixed at 10.0 mm. The 3.0 mm-in-thickness solid anode region is also included in the calculation domain with a simplified model to treat the anode sheath [15]. The width of the annular slot for the injection of the cold plasma-forming gas is 1.0 mm. The distance between the frontal surface of the shielding gas nozzle and the cathode tip ($L$) is varied in order to reveal its influences on the non-equilibrium features of the arc plasmas. The outer edge of the calculation domain is located 25.0 mm away from the arc axis in the

radial direction.

The boundary conditions used in this study are listed in Table 1. At the exit section of the shielding gas nozzle (JA), the radial velocity component ($v_r$) is assumed to be zero, while the $r$-dependent axial-velocity component ($v_z$) is assumed to have the form

$$v_z = v_0\left\{1-\left[2\left(r-1.5\right)/d\right]^2\right\} \qquad (11)$$

where $v_0$ is the maximum value of the axial velocity component and calculated from the total flow rate of the shielding gas. The distributions of the heavy-particle/ electron temperatures and the current density along the cathode surface are specified as the inner boundary conditions at the cathode-arc interface based on the model of the non-linear surface heating [10, 16, 17].

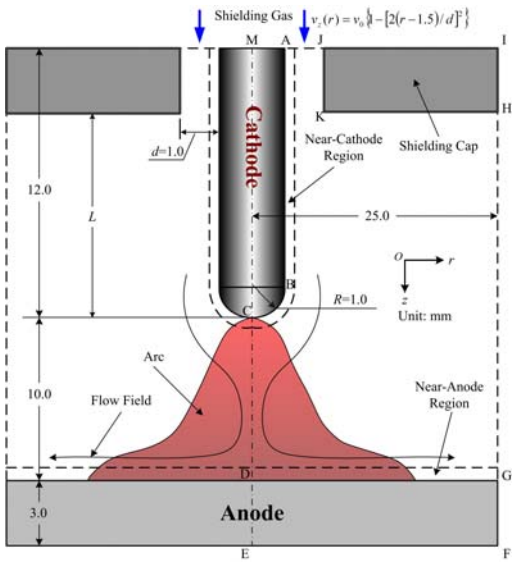


Fig. 1. Calculation domain.

## 3. Modeling results and discussion

In this study, the non-equilibrium features of the GTA plasmas are simulated by solving the Equations (1)-(5), (7)-(9) with the appropriate boundary conditions, and coupling with the non-linear surface heating model [10, 16, 17]. For the case with the arc current $I$=140 A, shielding gas flow rate $Q_{shield}$ =0.91 m$^3$/hr, and $L$=10.0 mm, the predicted electron and heavy-particle temperature distributions in the arc region are presented in Fig. 2. It can be seen that near the cold electrodes and in the arc fringes, $T_e$ is much higher than $T_h$, which shows a significant deviations of plasmas from LTE state. The corresponding temperature profiles along the arc axis are shown in Fig. 3.

Keeping other parameters, *e.g.* $I$ and $L$, being constant, it is found that the high temperature region of the arc becomes narrower with increasing $Q_{shield}$ due to the stronger cooling effects of the shielding gas on the arc, as shown in Figs. 4 and 5. It can be seen from Fig. 4 that the heavy-particle and electron temperatures increase at a higher shielding gas flow rate due to the pinch of the arc core region, and consequently, lead to a higher current density near the arc axis.

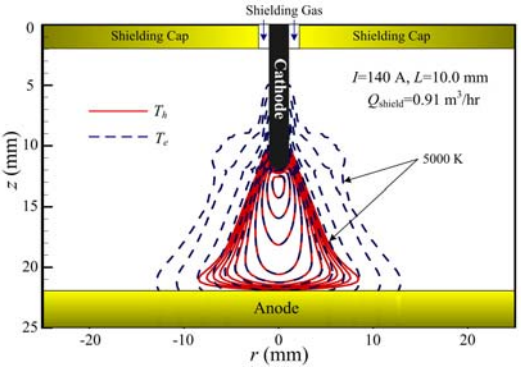


Fig. 2. Electron (dashed line) and heavy-particle (solid line) temperature distributions in the arc region.

(The outer isotherm is 5000 K with interval of 1000 K)

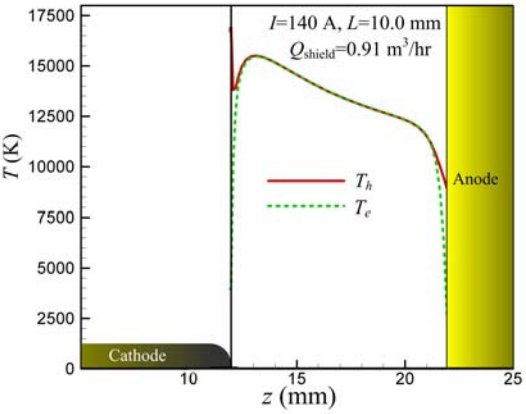


Fig. 3. Temperature profiles along the arc axis.

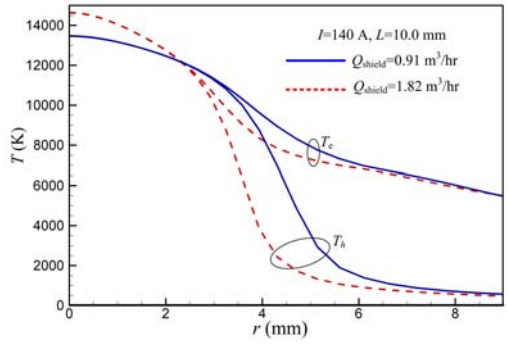


Fig. 4. Comparison of the radial temperature profiles at the mid-plane ($z$=17.0 mm) between the cathode and the anode for different shielding gas flow rates.

Similar calculated results are shown in Fig. 6 for different values of $L$ while keeping $I$ and $Q_{shield}$ being unchanged. Figure 6 shows that the high temperature region of the arc becomes narrower when the shielding-gas nozzle exit is closer to the anode (or the cathode tip), also due to the stronger cooling effect of the

shielding gas on the high temperature regions of the arc.

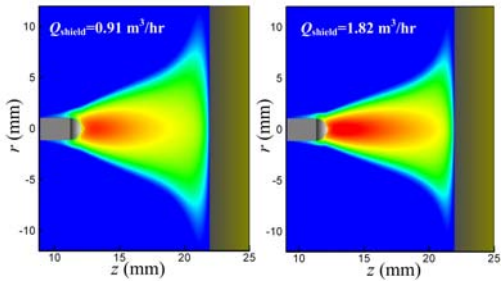


Fig. 5. Distributions of the heavy-particle temperatures in the arc region for different shielding-gas flow rates ($I$=140 A, $L$=10.0 mm, temperature range from 3000-16000 K).

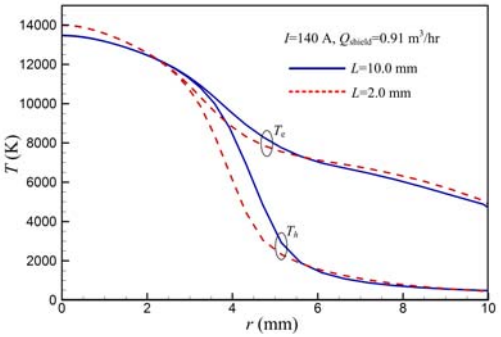


Fig. 6. Comparison of the radial temperature profiles at the mid-plane ($z$=17.0 mm) between the cathode and the anode for different locations of the shielding cap ($L$).

## 4. Conclusions

In this paper, a 2D, non-equilibrium modeling on the characteristics of the GTA is conducted with the consideration of the cathode sheath. The modeling results show that the shielding gas flow rates and the positions of the shielding gas nozzle exit have obvious influences on the non-equilibrium characteristics of the GTA plasmas, especially in the arc fringes.

**Acknowledgement** This work was supported by the National Natural Science Foundation of China (Nos. 10405015, 10710293), and by the project PPCDT/FIS/60526/2004 of FCT, POCI 2010 and FEDER (Portugal).

## References

[1] P. Fauchais and A.Vardelle, IEEE Trans. Plasma Sci. **25**, 1258 (1997).
[2] E. Gidalevich, S. Goldsmith and R. L. Boxman, Plasma Sources Sci. Technol. **13**, 454 (2004).
[3] M. Keidar and M. B. Schulman, IEEE Trans. Plasma Sci. **29**, 684 (2001).
[4] M. Keidar, J. Fan, I. G. Boyd and I. I. Beilis, J. Appl. Phys. **89**, 3095 (2001).
[5] J. Rosen and A. Anders, J. Phys. D: Appl. Phys. **38**, 4184 (2005).
[6] P. G. Jonsson, R. C. Westhoff and J. Szekely, J. Appl. Phys. **74**, 5997 (1993).
[7] S.-Y. Lee, and S.-J. Na, The Welding Journal (Supplement) **75**, 269 (1996).
[8] M. Ushio and F. Matsuda, Trans. JWM **11** (1), 7 (1982).
[9] J. F. Bott, The Physics of Fluids **9** (8), 1540 (1966).
[10] H.-P. Li and M. S. Benilov, J. Phys. D: Appl. Phys. **40**, 2010 (2007).
[11] D. M. Chen and E. Pfender, IEEE Trans. Plasma Sci., **PS-9** (4), 265 (1981).
[12] M. Mitchner and C. H. Kruger, Jr., Partially Ionized Gases, New York: Wiley, 1992.
[13] R. S. Devoto, Physics of Fluids **16** (5), 616 (1973).
[14] D. R. Lide, The CRC Handbook of Chemistry and Physics, the 83rd Edition, New York: CRC Press, 2003.
[15] X. Chen and H.-P. Li, Int. J. Heat Mass Transfer **44**, 2541 (2001).
[16] M. S. Benilov, J. Phys. D: Appl. Phys. **41**, 144001 (2008).
[17] M. S. Benilov, M. D. Cunha and G. V. Naidis, Plasma Sources Sci. Technol. **14**, 517 (2005).

**Table 1.** Boundary conditions for the modeling of the flow-affected region.

| | ABC | CD | DE | EF | FG | GH | HI | IJ | JA |
|---|---|---|---|---|---|---|---|---|---|
| $v_r$ | 0 | 0 | 0 | 0 | 0 | $\partial(\rho r v_r)/\partial r = 0$ | 0 | 0 | 0 |
| $v_z$ | 0 | $\partial v_z/\partial r = 0$ | 0 | 0 | 0 | $\partial v_z/\partial r = 0$ | 0 | 0 | Eq.(11) |
| $T_h$ | specified | $\partial T_h/\partial r = 0$ | $\partial T/\partial r = 0$ | 300 | 300 | $v_r$>0, $\partial T_h/\partial r = 0$; $v_r$<0, $T_h$=300 | 300 | 300 | 300 |
| $T_e$ | | $\partial T_e/\partial r = 0$ | / | / | / | $\partial T_e/\partial r = 0$ | / | / | 300 |
| $\phi$ | $j_n(s) = -\sigma(\partial\phi/\partial n)$ | $\partial\phi/\partial r = 0$ | $\partial\phi/\partial r = 0$ | 0 | $\partial\phi/\partial r = 0$ | $\partial\phi/\partial r = 0$ | $\partial\phi/\partial r = 0$ | $\partial\phi/\partial z = 0$ | $\partial\phi/\partial z = 0$ |